ENCIT2018-0138

ANALYSIS OF PRESSURE DISTRIBUTION GENERATED BY WIND LOAD IN AN ORE RECOVERY

Moisés de Paula Gouvea
Caio Almeida Friche Passos
Rubens Perdigão Diz Oliveira
Janes Landre Júnior
Cristiana Brasil Maia
Pontifícia Universidade Católica de Minas Gerais – Av. Dom José Gaspar, 500 Coração Eucarístico - 30535-901 - BH, Brasil
moisesgou@gmail.com
caio.friche@gmail.com
rubensperdigao@hotmail.com
janes@pucminas.br
cristiana@pucminas.br

Abstract: *Modeling and CFD simulation of pressure losses and air velocity in structures submitted to unilateral wind loads has been a subject widely covered in the automobile and civil industries. The mining field, which has large equipment working with large masses of ore submitted to wind loads can suffer from damage and sudden stop resulting in production losses. The objective of this work is the development of a numerical model of the flow around an ore recovery subjected to a critical speed load. The model was developed using the Ansys-Fluent software considering the conditions of steady state, air as an ideal gas and segregated flow. The velocity found in some spots around the ore recovery was 40% higher than the uniform velocity setup at the inlet, 60 km/h. A significant number of vortices were generated along the tunnel behind the recovery with a high range of velocities. The average static pressure found in the front of the recovery where the wind flux hits is around 200 Pa.*

Keywords: *pressure analysis, CFD, 3D modeling, mining equipment.*

.

1. INTRODUCTION

Brazilian history was strongly influenced by the exploitation of its mineral resources. The minerals and its metals always contributed to the supply of important inputs to the Brazilian industrial park, leveraging the national economy (Robles, 2012). Nowadays, the mining sector is responsible for a share of 5% of the Brazilian gross domestic product (GDP), which corresponds to about US$ 40 billion (IBRAM, 2015). Owing to its great economic importance, mining has traditionally attracted investments, generating thousands of jobs and boosting the country's development. However, the profitability of the mining sector is strongly dependent on its extractive activity, on the ability to move the ore from the field to the ports and on its boarding on ships.

Within this context, the maritime terminal of Tubarão, in Espírito Santo, with capacity to receive and load 120 million tons of ore per year and receive about 1.1 thousand ships with capacity for 400 thousand tons each per year, plays an important role in the logistics process of Brazilian mining (G1, 2018). Owing to strategic issues, maintaining the operating capacity is critical to the country’s and company’s economics health.

Large mining equipments play an important role in the flow of extracted minerals. They make it possible to operate at high productivity. The ore recovery stands out for having a capacity to recover up to 8 thousand tons per hour. The equipment is subjected to structural tensions during its work, generated by its own weight, ore movement through the ore track and it is also approached by gusts of winds that can reach the speed of 60 km/h in port regions (Pegorim, 2017).

Virtual simulation of structure, dynamics and fluids comes to help the project of new equipment and to prevent a sort of problems that could occur during the daily work. Computational Fluid Dynamics (CFD) is a type of virtual simulation in which the fluid and its interaction with the media is the point of study. Since 1930, with the development of the first methods to solve linearized potential equations with Navier Stokes formulations (Milne-Thomson *et al*., 1973), the CFD tool is rising and being more adopted to solve easy and complex problems in fluid-mechanic fields.

Wind load studies using the CFD technique have been performed approaching the effects of lateral winds on cyclists (Fintelman *et al*., 2015), road vehicles submitted to crosswinds (Tsubokura *et al*., 2010), the wind flow in sand dunes (Kim *et al*., 2015), the flux dynamics inside places (Zou *et al*., 2018), the wind loads on a container ship (Janssen *et al.*, 2017), the wind dynamics as a function of the positioning of doors and windows in houses (Peren *et al*., 2015), the impact of air flow lateral pressure on a bus (Zhu and Zhigang, 2015), the pressure generated at the top of elevated buildings (Zang *et al*., 2012), the pressure in lifting of loads subjected to winds (Han and Han, 2011), and the variation of uplift force in the support structure of a maritime container crane during a storm with high velocity winds (Han *et al.*, 2011).

These papers worked to describe the phenomenon and, at the same time, create the possibility to perform an improvement, like Peren *et al*. (2015), who attempted to deliver a better air flux modifying the position of the doors, windows and roof angle to increase air renewal and avoid hot spots inside the house. The author stated that there is a

significant importance in the way that the air flows and focuses on the structures. Zou *et al*. (2018) studied the indoor wind to understand the flow inside the environment and to improve the position of the walls and furniture to a better not forced indoor air cleaning. Tsubokura *et al*. (2010) and Zhu and Zhigang (2015) worked with automobiles. The former authors assessed a car and the later, a bus. The lateral face bigger than the frontal face creates a restriction to the lateral air, increasing the capability of a displacement and detachment during a lateral air blast, similar to what could occur with an ore recovery. Zhu and Zhigang (2015) also observed detachment of the bus starting from 10 m/s of lateral wind when the force generated by the pressure loss exceeded the friction.

Despite the great range of CFD studies regarding wind load, the study for mining equipment allocated to ports is part of a field that has not been approached yet, making the present work a great contribution to this area. Thus, the objective of this work was to analyze the distribution of steady state pressures on the structure of an ore recovery when subjected to a constant wind load of 60 km/h, based on a three-dimensional model. The recovery chosen for this work was located in the maritime terminal of Tubarão and is shown in Fig. 1. The Ansys-Fluent commercial code was used to solve the equations that describe the airflow characteristics.

Figure 1. Recovery model similar to the one assessed in this paper.

2. NUMERICAL METHODOLOGY

The three-dimensional model developed was created from the model of the recovery, provided by a large Brazilian mining company – Vale. It has approximate dimensions of 67 meters in length, 22 meters in width and 27 meters in height and was positioned in a rectangular wind tunnel as a control volume, with the dimensions respecting 8% locking (Fintelman *et al*., 2015), defined from the stipulated size for the equipment to be studied.

A lateral positioning was chosen owing to the higher moment of inertia that consequently generates higher losses of load and drag, providing a critical situation to the recovery structure, the focal point of this study. The fluid in the control volume was modeled as ideal gas; its properties were evaluated at a temperature of 15 °C, value commonly used in wind tunnels to experimental and virtual tests (Starccm+, 2018); relative humidity of air 75% to 85% (Vale, 2018); and atmospheric pressure of 1atm. Considering these conditions, the density of air assumed was 1.225 kg/m³ and the dynamic viscosity was $1.802\ 10^{-5}$ kg/m.s (Çengel, 2012).

The equations that describe the problem are the mass conservation equation, as in Eq. (1), and the linear momentum equation, as in Eq. (2), given by Versteeg and Malalasekera (2007):

$$\nabla \cdot \left(\rho \cdot \vec{v}\right) = 0 \tag{1}$$

$$\nabla \cdot \left(\rho \cdot \vec{v} \cdot \vec{v}\right) = -\nabla p + \nabla \cdot \left(\mu \left[\left(\nabla \vec{v} + \nabla \vec{v}^{T}\right) - \frac{2}{3} \nabla \cdot \vec{v} I \right] \right) + \rho \{\vec{g}\} \tag{2}$$

The three-dimensional, steady and random fluctuations of the properties, characteristics of the turbulent regime, require the application of a turbulence model. In the present study, the k-ε model was used, which works with the concept of turbulent viscosity, given by Eq. (3):

$$\mu_t = \rho C_\mu \frac{k^2}{\varepsilon} \tag{3}$$

where ρ, C_μ , k and ε represent, respectively, the specific mass, an empirical constant, the turbulent kinetic energy and the dissipation of the turbulent kinetic energy. Therefore, transport equations for the turbulent quantities given by Eq. (4) and Eq. (5) are required:

$$\frac{\partial}{\partial x_i}(\rho k u_i) = \frac{\partial}{\partial x_j}\left[\left(\mu + \frac{\mu_t}{\sigma_k}\right)\frac{\partial k}{\partial x_j}\right] + G_k + G_b - \rho\varepsilon - Y_M + S_k \tag{4}$$

$$\frac{\partial}{\partial x_i}(\rho \varepsilon u_i) = \frac{\partial}{\partial x_j}\left[\left(\mu + \frac{\mu_t}{\sigma_\varepsilon}\right)\frac{\partial \varepsilon}{\partial x_j}\right] + C_{1\varepsilon}\frac{\varepsilon}{k}\left(G_k + C_{3\varepsilon}G_b\right) - C_{2\varepsilon}\rho\frac{\varepsilon^2}{k} + S_\varepsilon \tag{5}$$

3. METHODOLOGY

The recovery geometry was loaded in the fluid dynamics software Ansys-Fluent® and passed through a geometry simplification in the Fluent subpack software named Fluent meshing® to create the first based mesh. During Janssen *et al*. (2017) study, different geometry models with the same physics symbolizing a container ship in a wind blast were tested and proved that in some conditions, well defined, the geometry could be simplified with blocks with medium definition returning results similar to those with higher definition. To run a CFD model as bigger as necessary to an ore recovery some simplifications should be done once the hardware capacity influence to run models with a bigger mesh. Thus, the recovery model passed through a box simplification as shown in Fig. 2 to turn capable to run in the hardware available. Ladders, randrails, steel cables and platforms that offers little resistance to the air were despised because they did not affect the final result. The first mesh results were in around 3 million elements.

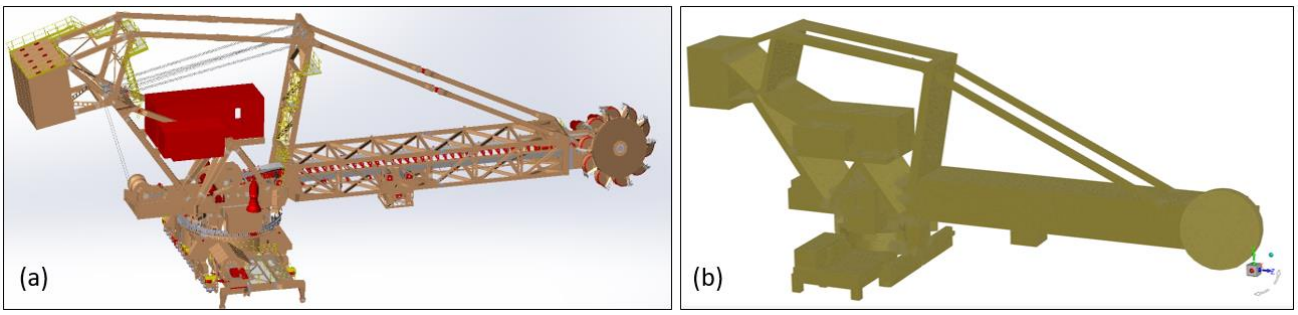

Figure 2. (a) Ore recovery geometry without cleaning; (b) Ore recovery with box cleaning and first mesh.

After that, the dimensions of the control volume were defined according to the Fluent datasheet best practices (Fluent, 2017), that composes the virtual wind tunnel dimensions based on the geometry proportions of the instrument of study, as it can be seen on Figure 3.

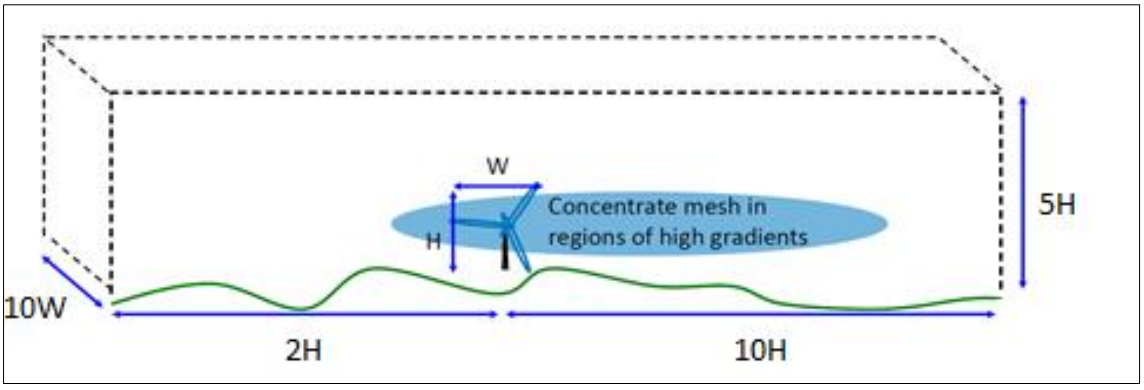

Figure 3. Configuration of the wind tunnel (Fluent, 2017).

The wind tunnel was assembled with the geometry of the ore recovery with the contact between the ground and the ore recovery feet. A second surface mesh was done with mesh treatment reducing the mesh to around 300000 elements, maintaining the geometry form and mesh necessary quality. This surface mesh drop is caused by the restraint of the mesh treatment because the software creates the blocks without mesh patterns.

The fluid zone was detached from the surface mesh created and a volumetric mesh was generated in the defined control domain. The resulting volumetric mesh was carried to Fluent main program to define the boundary conditions, physics and preprocessing of the results.

The physical models applied were based on steady state simulation. The air was applied with constant density and dynamic viscosity in the temperature of 15 °C, assuming that through a costal storm the mandatory wind that blows the maritime courtyard happens with negligible variation. It was assumed the airflow in turbulent regime, since the air that shocks with the recovery detaches the formed boundary layer and, for a considerable distance, generates backyard vortices. For this case, the turbulence model k-ε was used to model the external flow and SIMPLE scheme method was used to determine the coupling between pressure and velocity, as in recent works, like Fintelman *et al*. (2015), Zhu and Zhigang (2015) and Han and Han (2011).

Figure 4 shows the setup of the virtual tunnel. The front face in red was configured as velocity inlet with a constant value of 60 km/h (16.67 m/s). The lateral walls and the ceiling were configured as symmetry planes. The outlet face in blue was defined as relative pressure equal to zero and the floor was configured as a non-slip surface, as well as the equipment.

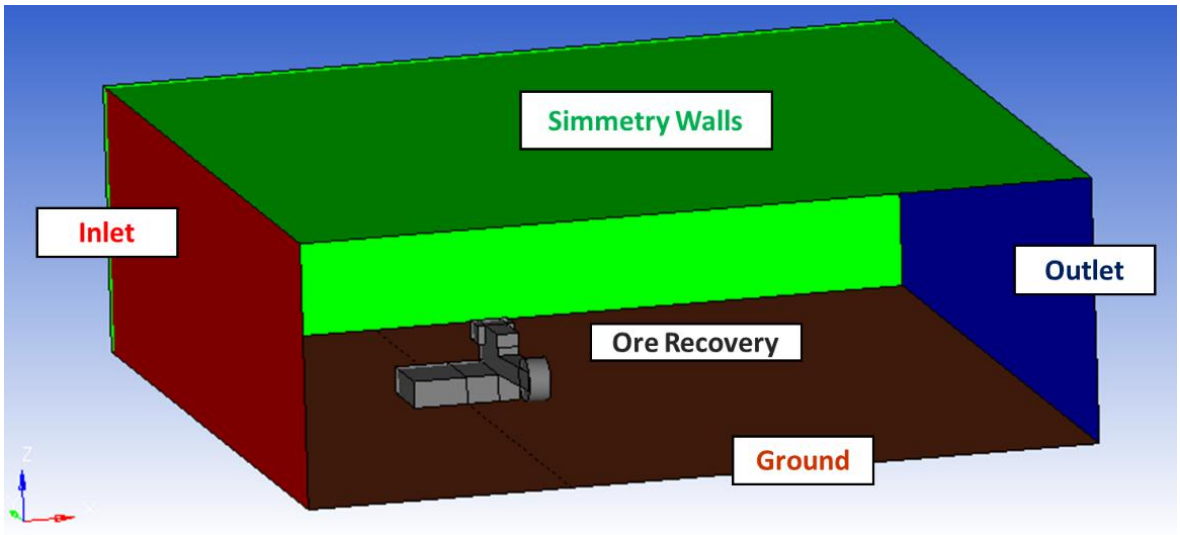

Figure 4. Configuration of the wind tunnel.

Predicting turbulence after the recovery structure, two box refinements, one smaller and other one bigger, with high and medium refinements, were done (Fig. 5) to analyze the vortex phenomenon.

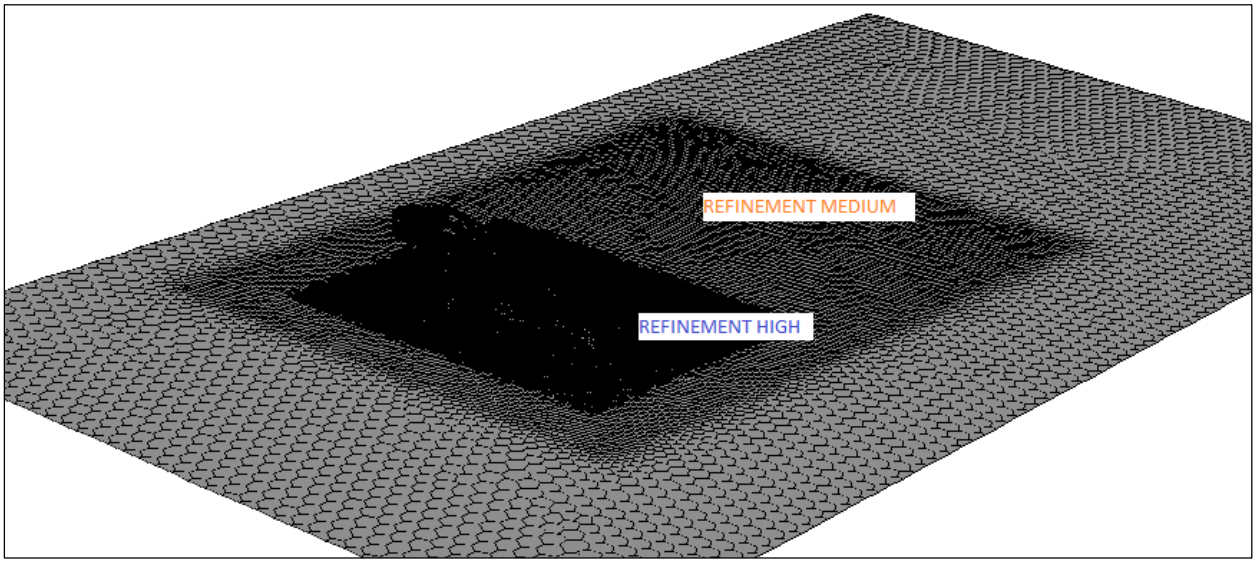

Figure 5. Configuration of the wind tunnel.

Mesh tests were performed with tetrahedral and polyhedral mesh. The difference between them is that polyhedral mesh presents less cell count and higher number of faces of each element, which accommodates better the geometry, performing a better contact between the cells (Fluent, 2017). It was assumed polyhedral mesh because it performs a better convergence with less floating of the monitored points, despite the time cost for each iteration increases.

In order to obtain more accurate results close to the wall, it is necessary to check the Law of the Walls, defined by von Karman (1930), which determines the average velocity of a turbulent flow in a fluid region near the wall. For this, the value of de dimensionless parameter Y+ (Eq. 6), (Schlichting and Gerstein, 2000), was used as the evaluation criterion.

$$y+ = \frac{\Delta y * Ut}{\nu} \tag{6}$$

Where Δy is the distance from the wall, Ut the friction velocity and ν the kinematic viscosity.

To ensure a good convergence, Y+ must be within the acceptable range, between 30 and 300, using wall functions and working in turbulent logarithmic region (Fluent, 2017; Schlichting and Gerstein, 2000). Considering a Y+ around 200, the distance from the wall about 300 mm and a velocity around 16 m/s, the estimated Δy is about 5mm. Twelve prism layers were created in the ore recovery with a scaled growth to conform the tunnel mesh with the prism mesh.

A coarse, a medium and a refined mesh tests were done for the proposed model. Table 1 shows the mesh configurations.

Table 1. Mesh sizes for mesh testing.

Mesh Type	Mesh Size (mm)	High Refinement Box (mm)	Medium refinement Box (mm)	Tunnel Refinement (mm)	Volume elements
Coarse	600(max)	1500(max)	3000(max)	5000(max)	900 thousand
Medium	300((max)	900 (max)	2000(max)	5000(max)	2.7 million
Refined	150(max)	350(max)	1000(max)	3000(max)	6.8 million

The mesh test consisted in running the three models with different meshes until the residues and a monitored point (Fig. 6 - in yellow) stabilized. The yellow point of the figure was chosen because it is a detachment region, where was expected a velocity increase and to appear turbulence vortices.

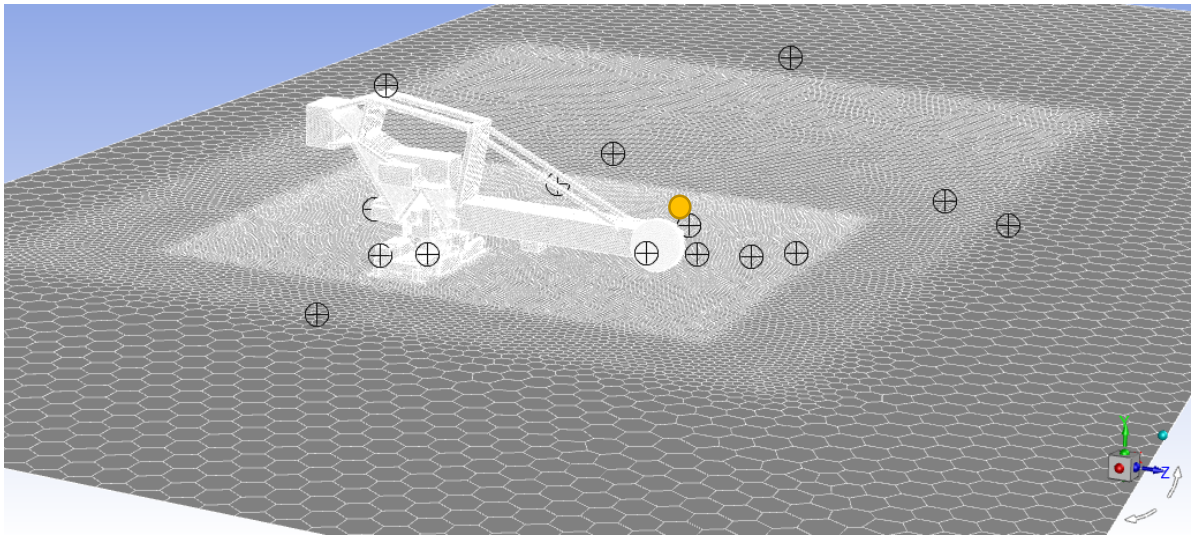

Figure 6. Monitoring points on the ore recovery and wind tunnel.

The medium polyhedral mesh (Fig. 7) was adopted because it offered a better time per iteration than the refined one, once the number of elements turns the iteration process substantial, and presented a good convergence, with a value floating in about 3% of the pressure and velocity monitored, whereas the refined mesh presented around 2% floating.

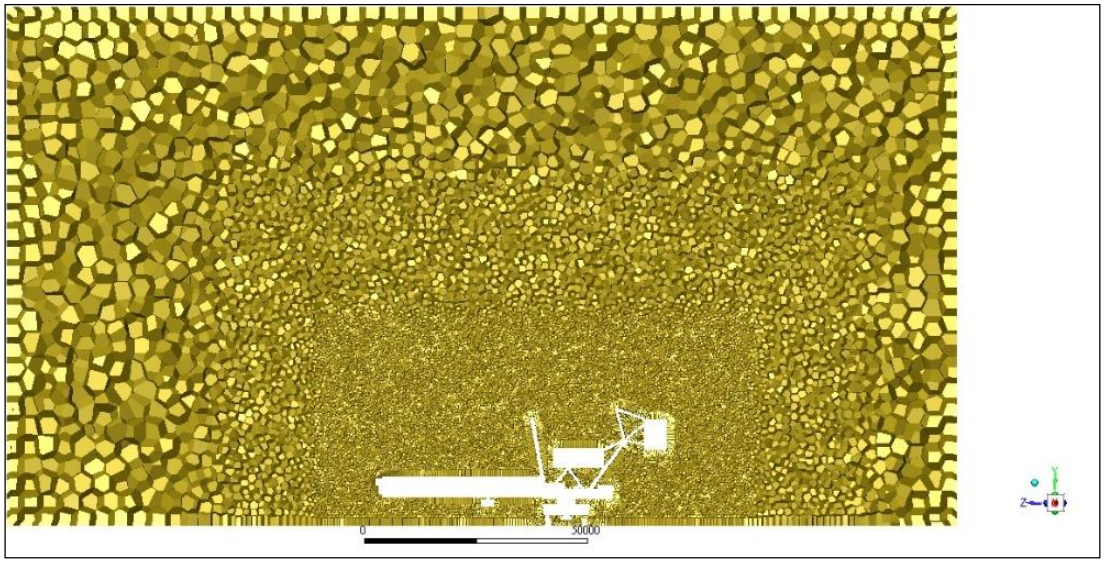

Figure 7. Final polyhedral mesh with refinements applied. Cut in plane y x z.

Key points around the recovery and in different parts of the wind tunnel were placed (Fig. 7) to monitor pressure and velocity during the iteration and they will be discussed. The possibility of an accident or a malfunction caused by that high pressure and velocity will also be debated. Residues between 10^{-4} and 10^{-5} were guaranteed. It was expected that the model obtained convergence around 2000 ~ 5000 iterations (Fintelman *et al*., 2015; Peren *et al*., 2015). As the model did not involve temperature variations, the energy equation was not solved, and the expected results were pressure and velocity in the airflow around the ore recovery and its structure.

4. RESULTS AND DISCUSSIONS

The residues stabilized between 10^{-3} and 10^{-5} after one thousand and five hundred iterations. To process all the 2.8 million polyhedral mesh running in a core i7 7700HQ laptop with 16gb of memory about 3 hours were required. The Y+ average value found were around 220, as expected.

After the iteration process ended and the convergence of the model was confirmed, the results were taken. As expected, the accelerated fluid touched the asymmetric and big sized ore recovery structure, generating a pressure loss, a long vortex patch (initiating from the disruption point), and a velocity increase in the sides and in the geometry convergence regions, as seen in Fig. 8, that shows the velocity magnitude field in a y plane.

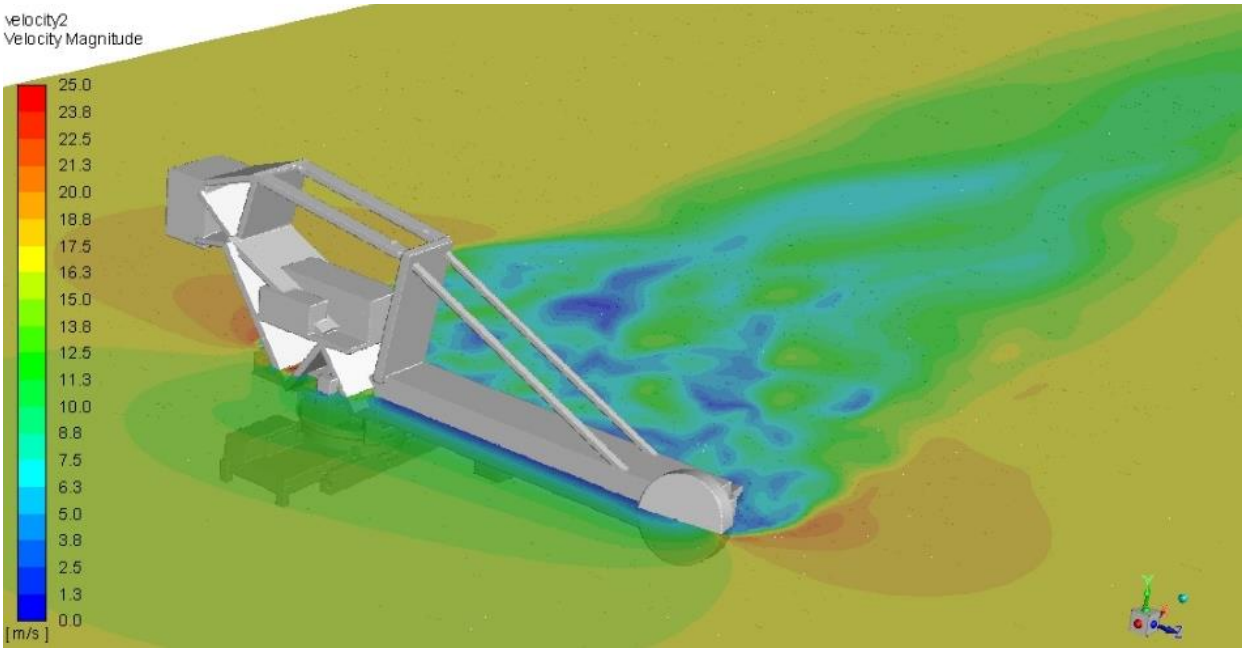

Figure 8. Velocity magnitude results of the ore recovery model, cut in y.

As in Figure 8, Figure 9 shows the velocity result in y cut, but in different positions: one in the ore recovery feet (a), and the other in the ore recovery top (b). It is possible to see the difference in the velocity profiles generated by the dynamic of the air passing through the structure acting like a torch. The accelerated air from the sides creates a curtain that traps the low speed air profile from the recirculation voids only behind the bigger-sized geometry. The profile of the vortices is mainly linked with the geometry and detachment. In addition, comparing the cuts of Fig. 8 and Fig. 9, it is possible to notice that the bigger the geometry blockage, the more often is the occurrence of places with velocity close to zero. The highest velocity spot was found in the places between the ground and the ore recovery geometry (Fig. 9a).

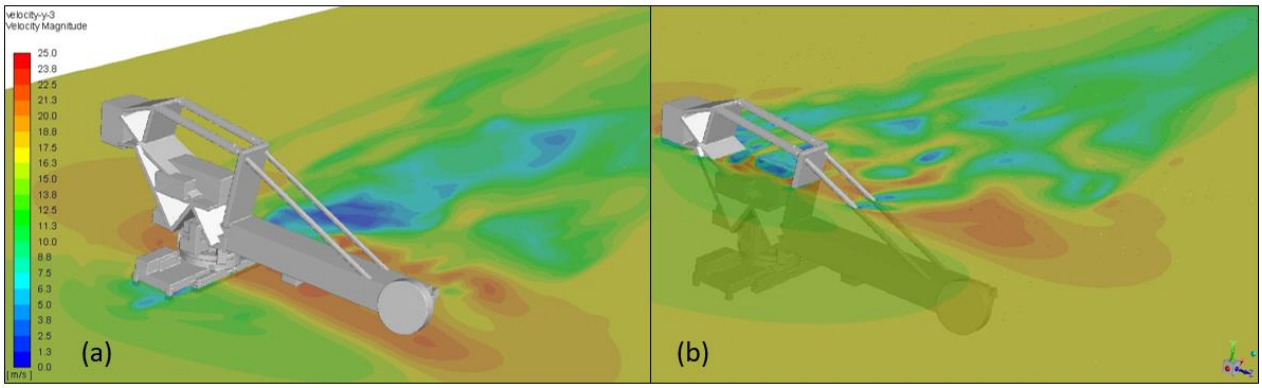

Figure 9. Velocity magnitude results of the ore recovery model: (a) Cut in y positioned on the ore recovery feet; (b) Cut in y positioned on ore recovery top.

Figure 10 presents the velocity magnitude in a x plane cut represented by pathlines. An important thing to notice is that the inlet velocity setup is about 16.7 m/s (60 km/h) and it rises to 24.5 m/s (86.5 km/h) in some areas on the side of the recovery and on its leaked spots. As estimated, the regions close to the ground, with structures assembled pierced to the other side and around the equipment presented a velocity increase.

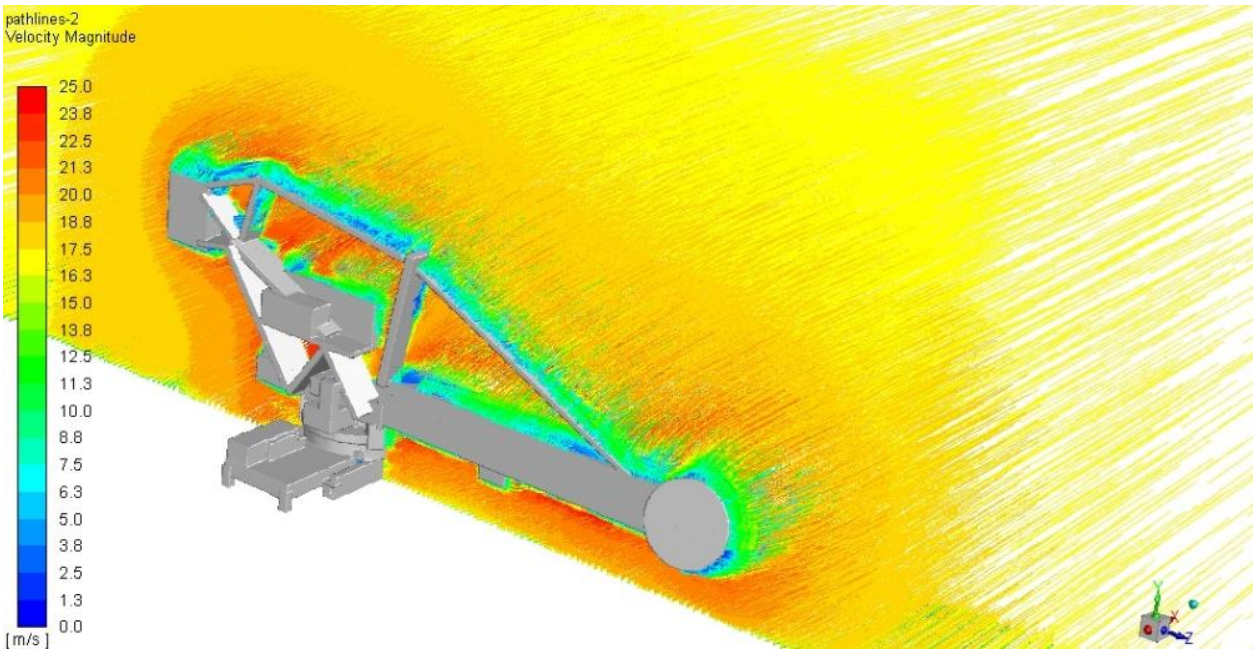

Figure 10. Velocity magnitude results of the ore recovery model, cut in x represented by pathlines.

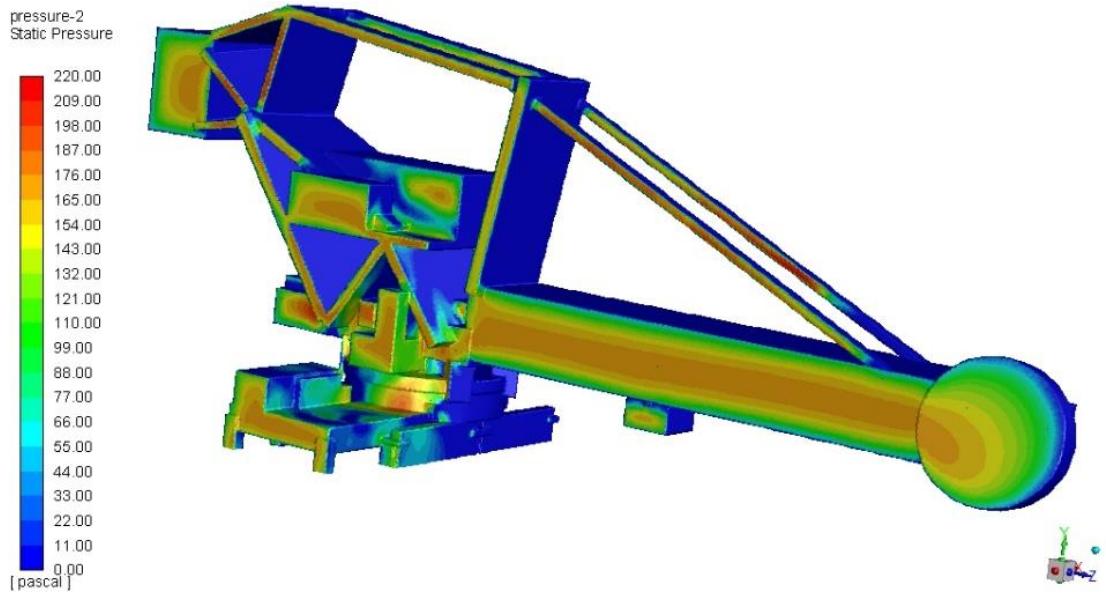

Figure 11. Static pressure results of the ore recovery model.

For the turbulence area behind the recovery and close to the flow detachment it is possible to see recirculation zones with velocity close to zero. The region close to the front of the recovery area also has zero velocity regions, which is caused by the air escaping from the surface zone. This phenomenon increases the pressure in some places, as can be seen in Fig. 11.

The maximum pressure value obtained was 265 Pa, found close to the basis part. It was found there probably because it is the deeper region to the air flow passage, close to the gravity center, where all the contents of the ore recovery are connected, creating a high concentration of mass and deceleration spot.

The maximum velocity value found was 24.8 m/s, on the place above the long structure called spear, which accommodates the ore mat and assemblies the bucket wheel. Probably the faster place was found there because it is the longer part and so it increases the velocity profile by creating a huge barrier.

The static pressure distribution over the area that is receiving the flow is uniform and around 200 Pa. Despite the value being harmless to a heavy weight and large machine, the distribution of 200 Pa is not punctual, the air flow works oscillating its velocity value and the ore recovery is mounted on rails only on its basis. As the recovery has a large area with 67 m length by 27 m high, the pressure force could displace and/or twist the equipment structure under specific conditions. As the results show, it is easier to the recovery submitted to the wind to twist and be carried by the wind to the ground or through the grills than directly topple because the frictional force between the structure and the rail could be overcome by the momentum of the lever arm formed by the large spear structure and its basis.

5. CONCLUSIONS

This paper was motivated by the necessity to understand the phenomena of the wind shock in equipments that work in harbors. The model based in the real geometry of an ore recovery from Vale company was created by replacing all the original geometry parts for blocks to simplify and reduce the number of elements. Thus, the cleaned geometry was assembled in a wind tunnel and a polyhedral volumetric mesh was shaped. A mesh test with different sizes of meshes was performed and the medium mesh was chosen to run the tests, since the results of the residuals and the monitored points were in an acceptable level of convergence. Also the medium geometry offers a better time per iteration than the refined one, once the number of elements turns the iteration process substantial.

By the analysis of the results, it was concluded that the resultant velocity in the structure of the ore recovery by entering with a 60km/h uniform wind input in inlet could be 40% higher in some leaked spots and structure corners, where the wind escapes. As expected, the turbulence generated created vortices behind the recovery with a large profile of velocities, which, in some places, was close to zero, like the face that receives the wind-blown. It was caused by the instant decrease of the air velocity, creating a pressure rise and accelerating the air in the corners, where the air has space to scape.

The static pressure profile found in the frontal area pointed to the flow presented a uniform distribution around 200 Pa. Despite not being a high value of pressure, owing to the large size of the equipment, the work position and the momentum of the structure geometry, this pressure can generate a large force, which could propitiate a lever arm to the ore supports to the ground and possibly cause structure twist and displacement under specific conditions and even drag the recovery along the rails or to the ground by overcoming the frictional force between the trail and the recovery basis.

6. ACKNOWLEDGEMENTS

The authors thank Vale, PUC Minas, FAPEMIG, CAPES and CNPq for their financial support.

7. REFERENCES

Çegel, Y. A. and Ghajar, A. J., 2012. *Transferência de calor e massa: uma abordagem prática*. Ed AMGH, Porto Alegre, 2nd ed.

Fintelman, D., Hemida, H., Sterling, M. and Li, F., 2015. "CFD simulations of the flow around a cyclist subjected to crosswinds". *Journal of wind engineering and Industrial Aerodynamics*, Vol. 144, p. 31-41.

Fluent, 2017. "Datasheet and Help". March 2017, version 19. Available only for computers with the software installed.

G1, 2018. "Porto de Tubarão faz 50 anos e é responsável por 13% do PIB do ES". 25 Jul. 2018. <http://g1.globo.com/espirito-santo/noticia/2016/04/porto-de-tubarao-faz-50-anos-e-e-responsavel-por-13-do-pib-do-es.html>.

Han, D. and Han, G., 2011. "The difference in the uplift force at each support point of a container crane between FSI analysis and a wind tunnel test". *Journal of Mechanical Science and Technology*, Vol. 25, p. 301-308.

Han, D. and Han, G., 2011. "The difference in the uplift force at each support point of a container crane between FSI analysis and a wind tunnel test". *Journal of Mechanical Science and Technology*, Vol. 25, p. 301-308.

Han, D., Yoo, S., Yoon, H., Kim, M., Kim, S. and Lee, J., 2011. "Coupling analysis of finite element and finite volume method for the design and construction of FPSO crane". *Automation in Construction*, Vol. 20, p. 368–379.

IBRAM, 2015. *Informações sobre a economia mineral brasileira 2015*. Instituto Brasileiro de Mineração, Brasília, 1st ed.

Janssen, W.B., Blocken, B. and Wijhe, H.J., 2017. "CFD simulations of wind loads on a container ship: Validation and impact of geometrical simplifications". *Journal of Wind Engineering and Industrial Aerodynamics*, Vol. 166, p. 106-116.

Kim, H., Jeong, C. and Huh, S., 2015. "FSI Analysis and Fatigue Analysis of BOP Gantry Crane". *Advances in Mechanical Engineering*, Vol. 7, p. 347-358.

Milne-Thomson, L.M., 1973. *Theoretical Aerodynamics*. Dover Publications.

Pegorim, J., 2017. "Por que o vento aumentou no litoral sul e sudeste". 12 Dez. 2017. <https://www.climatempo.com.br/noticia/2017/10/31/por-que-o-vento-aumentou-no-litoral-do-sul-e-do-sudeste--2104>.

Peren, J.I., van Hoff, T., Leite, B.C.C. and Blocken, B., 2015. "CFD analysis of cross-ventilation of a generic isolated building with asymmetric opening positions: Impact of roof angle and opening location". *Building and Environment*, Vol. 85, p. 263-276.

Robles, L.T., Alcântara, M.B. and Cutrim, S.S., 2012. "Eficiência Global da Operação Portuária: estudo de caso do Píer I do Porto de Tubarão em Vitória-ES". *Revista Organizações em Contexto*-online, Vol. 8, p. 195-221.

Schilichting, H and Gersten, K., 2000. *Boundary-Layer Theory*. Ed Springer, Bochum, 8th ed.

Starccm+, 2018. "Datasheet and Help". March 2018, version 12.04.009. Available only for computers with the software installed.

Tsubokura, M., Nakashima, T., Kitayama, M., Ikawa, Y., Doh, D. and Kobayashi, T., 2010. "Large eddy simulation on the unsteady aerodynamic response of a road vehicle in transient crosswinds". *International Journal of Heat and Fluid Flow*, Vol. 31, p. 1075-1086.

Vale, 2018. "Regulamento do terminal maritimo de ponta da madeira." 13 Mar. 2018. < http://www.vale.com/PT/business/logistics/shipping/ship_tracking/Documents/regulamento_terminal_ponta_madeira-PT.pdf>.

Versteeg, H.K. and Malalasekera, W., 2007. *An Introduction to Computational Fluid Dynamics – The Finite Volume Method*. Pearson Education Limited, Edinburgh Gate Harlow, 2nd ed.

von Kármán, T., 1930. "Mechanical Similitude and Turbulence", Technical Memorandus NACA, no. 611.

Zang, Y., Borna, A., Khurram, R. and Habashi, W., 2012. "Hybrid RANS/LES method for FSI simulations of tall buildings. Advances in Civil, Environmental, and Materials Research". *The 2012 World Congress on Advances in Civil, Environmental, and Materials Research (ACEM' 12).*

Zhu, H. and Zhigang, Y., 2015. "Fluid–structure interaction study of three-dimensional vehicle model under crosswind". *Advances in Mechanical Engineering*, Vol. 7, p. 1-10.

Zou, Y., Zhao, X. and Chen, C., 2018. "Comparison of STAR-CCM+ and ANSYS Fluent for simulating indoor airflows". *Build Simul,* Vol. 11, p. 165–174.

8. RESPONSIBILITY NOTICE

The authors are the only responsible for the printed material included in this paper.